Please cite as

Chen, Xiao; Tian, Zhao F; van Eyk, Philip J; Lewis, David; Nathan, Graham 'Gus' J

Experimental and Computational Multiphase Flow , 2022, Vol.4(2), p.113-120

Numerical simulation of hydrothermal liquefaction of algae in a lab-scale coil reactor

Xiao Chen[1], Zhao F. Tian[1], Philip J. van Eyk[2], David Lewis[2], Graham 'Gus' J. Nathan[1]

1. School of Mechanical Engineering, Center for Energy Technology (CET), the University of Adelaide, SA. 5005, Australia

2. School of Chemical Engineering & Advanced Materials, The University of Adelaide, Adelaide, South Australia 5005, Australia.

✉ Corresponding author's name and email address

Dr Zhao Tian, zhao.tian@adelaide.edu.au

Abstract: A computational fluid dynamics (CFD) model of a coil type hydrothermal liquefaction (HTL) reactor with feedstock of algae has been developed using reaction kinetics reported in the literature. The CFD model is applied to understand the effects of thermal conductivity, heat capacity, molar mass, and viscosity of both the reactants and products on the HTL reactions in terms of residence time and mass fractions, for this coil reactor. It is found that the heat conductivity, heat capacity and molar mass have negligible effects on the HTL reaction in this reactor. However, the viscosity, particularly of the dominant reactants such as the protein, was found to have the most significant effect on the residence time and mass fractions, particularly when the viscosity of protein is reduced from values of the base case. This highlights the need for better measurements of viscosity in future work.

Keywords: computational fluid dynamics, hydrothermal liquefaction, algae

1 Introduction

Hydrothermal liquefaction (HTL) is one of the engineering methods being developed to convert complex organic feedstock such as algae (Chiaramonti et al., 2017) into valuable products such as transport fuels and their precursors. However, the technology is not yet economically viable at commercial scale, due largely to outstanding scientific and technological challenges (Elliott et al., 2015). Of the many challenges, one is that the flow field, heat transfer and reactions in the HTL reactor are not well understood, partially due to the difficulties in obtaining reliable experimental measurements of the velocity field, temperature field and component concentration (e.g. the volume fraction of microalgae cells in an algae HTL process (Fu et al., 2018)) in the challenging environments of a reactor. However, the rapid increase in computing capacity, has led to computational fluid dynamics (CFD) being widely employed to investigate the heat transfer and reactions in a wide range of related chemical processes, such as the multiphase flows in pipes (Hu et al., 2020), combustions (Tian et al., 2017) and solar reactors (Chinnici et al., 2019). Compared with experimental approaches, CFD models are generally fast and low-cost (Yeoh & Tu, 2019), and can provide high-resolution results, such as velocity and pressure fields, temperature field and species volume fractions in reactors, and therefore are a promising research and design tool for HTL reactors (Obeid et al., 2019). In this paper, the latest progress of the CFD research on a coil HTL reactor conducted in the Center for Energy Technology (CET) at the University of Adelaide is reported.

Compared with the large number of experimental studies of HTL reported in the literature, for example in (Chiaramonti et al., 2017; Eboibi et al., 2015), there are few CFD models of these reactors, and these models employ many simplifications to reduce physical and chemical complexity. In the study of Tran et al. (2017), a CFD model of fast hydrothermal liquefaction was developed by employing the CFD package FLUENT. In this CFD model, cold and hot water streams, which were used as the surrogate of the HTL slurry, flowing and mixing in a 3D pipe domain were simulated to calculate the residence time distribution (RTD), the mixing and heat transfer in the reactor. Obviously, the components of the HTL slurry including feedstock and products, and HTL reactions were not included the surrogate model, which limits the applicability of this surrogate model. Fu et al. (2020) developed a CFD model of the microalgae slurry flow in a hydrothermal pre-treatment system using the CFD package FLUENT as well. The heat transfer in this solar-driven system was modelled. In this CFD model, the microalgae slurry flow was treated as a single phase material that is a mixture of water and microalgae cells. The properties of the slurry including density,

conductivity, and specific heat capacity in this model were constants obtained from experiments. Nevertheless, similar to the work (Tran et al., 2017), no chemical reactions were considered in this study.

In a later study, Chen et al. (2020) added reactions in the CFD model of Fu et al. (2018) and simulated the hydrothermal conversion of the microalgae slurry in a pipe flow model. Nevertheless, only the dissolution of carbohydrate and proteins were included in this simple reaction model, which is a great simplification of the complex reactions found in algae HLT processes. Ranganathan and Savithri (2018) developed a CFD model to simulate HTL of microalgae in a lab-scale continuous plug-flow reactor using the commercial package COMSOL. In this 2D unsteady CFD model, the algae slurry was modelled as a liquid mixture and the reaction of HTL was based on the pathway of a general kinetic model of HTL (Valdez et al., 2014). The simulated slurry temperature and the yield of HTL products were validated against experimental data by (Billing et al., 2016) and (Patel & Hellgardt, 2015), respectively. The agreement of the simulated temperature field with the measurement is satisfactory, while the simulated yields of products including biocrude, gas, and particularly the water-soluble deviate from the experiments by more than 10%. This deviation was attributed to the 2D CFD domain that cannot appropriately model the 3D flow and reactions, the kinetic model, and modelling of the slurry by a single phase mixture (Ranganathan & Savithri, 2018).

These previous CFD models of HTL processes with reactions modelled (Chen et al., 2020; Ranganathan & Savithri, 2018) were all undertaken in a 2D domain. There are no reported CFD studies with HTL reactions for the algae HTL reactors that have strong 3D flow features, such as the coil type HTL reactor developed in the Center for Energy Technology (CET) at the University of Adelaide shown in Figure 1, which is configured for potential application within a combustion chamber or with a solar receiver, e.g. the Solar Expanding-Vortex Particle Receiver (SEVR) (Chinnici et al., 2016). A comprehensive 3D CFD model is essential to understand the flow, heat transfer and reactions within such a coil reactor, to identify the preferred reactor configuration, and to optimise its design and operation. Nevertheless, significant uncertainties in the CFD models remain, such as insufficient information about the the heat capacity, thermal conductivity and viscosity. Therefore, an analysis of the sensitivity of the performance of the HTL process to these various parameters is needed to guide the development. In this paper, a CFD model of the HTL coil reactor has been developed by employing the CFD package ANSYS/CFX and applied to investigate the sensitivities of viscosity, heat capacity, heat conductivity, and molar mass of the components of the HTL slurry

on the reactions and residence time in the coil reactor. This information will guide the further development of the technology.

2 Methodology

A coil type vessel using stainless steel tube was adopted as the reactor for the current study, which was also designed for future experimental work. Fig. 1 presents the geometry and dimensions of the reactor, which comprises three components, i.e. an inlet pipe, a reactor vessel and an outlet pipe, as shown in Fig. 2. ANSYS meshing 18.0 was adopted for the generation of mesh. The sensitivity of the model to the computational grid size for predictions of the mass fractions of the ash-free algae solid, biocrude, aqueous-phase products and the gas product has been tested using meshes with 0.8, 1.7 and 3.2 million nodes, respectively. It shows that further refinement of the mesh from that with 1.7 million nodes to 3.2 million nodes does not significantly affect the predicted mass fractions. A mesh with 1.7 million nodes was thus adopted for the current work.

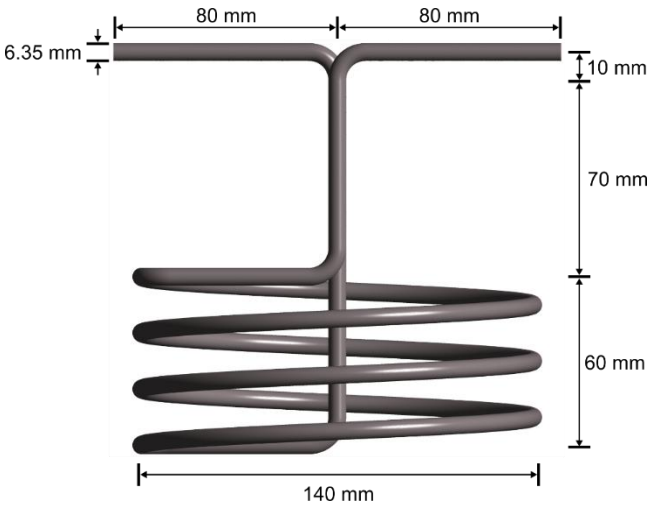

Fig. 1 The geometry and dimensions of the coil reactor investiated here.

The software ANSYS CFX 18.0 was chosen to conduct the steady-state simulation. The inflow is a 35 wt% slurry of Nannochloropsis sp. in water, with a continuous inlet velocity of 0.0018 m/s and a pressure of 20 MPa. The root-mean-square (RMS) of the residuals were all lower than 1×10^{-6} and the "High Resolution" numerical scheme was adopted for the advective terms.

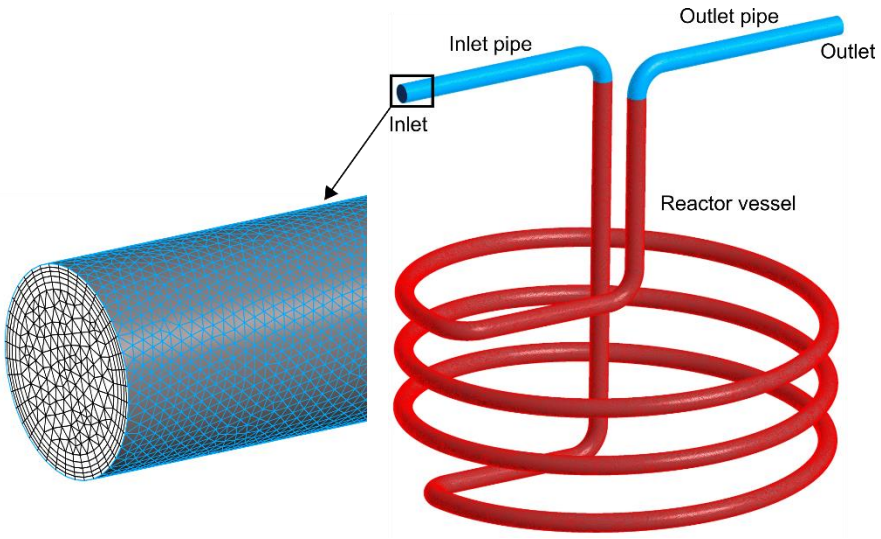

Fig. 2 Mesh of the current model

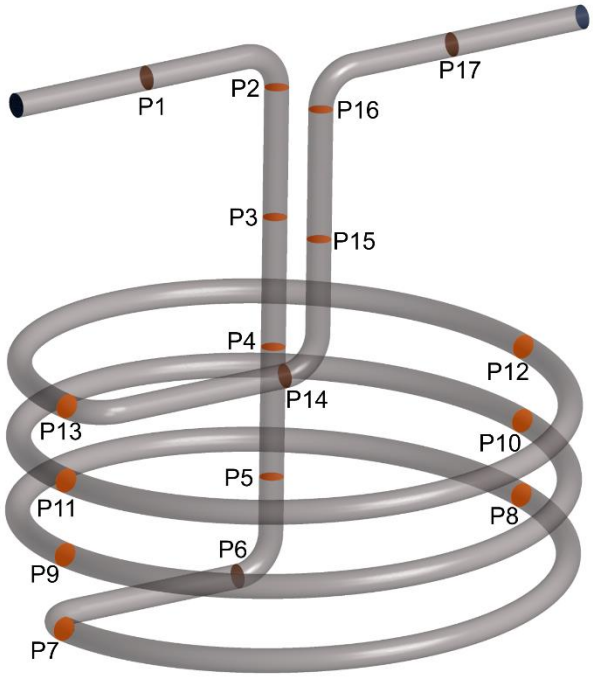

Fig. 3 Geometry of the coil reactor showing the locations of the sampling plans.

The temperature of the inflow was 25 °C, which is the assumed ambient temperature in the simulation. Here the outer surfaces of the inlet and outlet pipes were modelled being exposed to the ambient air, while the reactor vessel was assumed to be placed within a fluidised bath heater with a temperature of 300 °C. According to the work of Valdez et al. (2014), the inflow slurry is comprised of protein, carbohydrate, lipid and ash, with a dry-basis mass fraction of 56%, 32%, 9% and 3%, respectively. Products of this reaction are biocrude, gas and aqueous-phase products. The

main component of carbohydrate, protein, lipid, aqueous-phase and bio-crude products are glucose (Biller & Ross, 2011), albumin (Biller & Ross, 2011), glycerol (Barreiro et al., 2013), 2-pyrroldinone (Jena & Das, 2011) and heptadecane (Ross et al., 2010), respectively, while the main product gas is carbon dioxide (Barreiro et al., 2013). The relevant properties of both water and carbon dioxide at 300 °C and 20 MPa were obtained from the NIST Chemistry WebBook (2005), as shown in Table 1. Properties at 300 °C and 1 atm were adopted for the other materials in the algae HTL reactions, due to the lack of data at other conditions. The sensitivities of these properties on the predicted residence time over distance and the variation of mass fraction of ash-free algae solids, aqueous-phase products, biocrude and gas over time were studied in the current work, as shown in Table 2.

Table 1: Reference properties of the inflow and products components in the algae HTL reactions.

Material	Main component	Density (kg/m^3)	Molar mass (kg/kmol)	Heat capacity (J/kg·K)	Thermal conductivity (W/m·K)	Viscosity (kg/m·s)
Carbohydrate	Glucose (Biller & Ross, 2011)	1540	180	1214.4	0.487	2.91×10^{-3}
Proteins	Albumin (Biller & Ross, 2011)	996	67000	1276.97	0.45	6.85×10^{-2}
Lipids	Glycerol (Barreiro et al., 2013)	1039.3	92	3441.28	0.3245	3.11×10^{-4}
Aqueous-phase products	2-pyrroldinone (Barreiro et al., 2013)	850.419	85	2738.22	0.128	2.6×10^{-4}
Biocrude	Heptadecane (Ross et al., 2010)	568.199	240	3144.96	0.968	1.8×10^{-4}
Gas	Carbon dioxide (National Institute of Standards and Technology, 2005)	191.97	44	1245.6	0.047	3.39×10^{-5}
Water	Water	734.7	18	5316	0.57	9.01×10^{-5}

Table 2: Cases assessed in the sensitivity study of the properties of five components in the HTL reaction, relative to the reference values in Table 1.

	Thermal conductivity			Heat capacity			Molar mass			Viscosity		
Proteins	× 1/3	× 1	× 3	× 1/3	× 1	× 3	× 1/3	× 1	× 3	× 1/10	× 1	× 10
Carbohydrates	× 1/3	× 1	× 3	× 1/3	× 1	× 3	× 1/3	× 1	× 3	× 1/10	× 1	× 10
Lipids	× 1/3	× 1	× 3	× 1/3	× 1	× 3	× 1/3	× 1	× 3	× 1/10	× 1	× 10
Biocrudes	× 1/3	× 1	× 3	× 1/3	× 1	× 3	× 1/3	× 1	× 3	× 1/10	× 1	× 10
Aqueous-phase products	× 1/3	× 1	× 3	× 1/3	× 1	× 3	× 1/3	× 1	× 3	× 1/10	× 1	× 10
Gas	× 1/3	× 1	× 3	× 1/3	× 1	× 3	× 1/3	× 1	× 3	× 1/10	× 1	× 10

Fig. 4 presents the reaction kinetics adopted for the current simulation, following the work of Valdez et al. (2014). Reactants in the HTL reaction are considered to be protein, carbohydrates and lipids while products are biocrudes, aqueous-phase compounds and gas. The variation of mass fraction of each component in the reaction over time are shown in Equations 1-6,

Protein: $\frac{dx_{1,p}}{dt} = -\left(k_{1,p} + k_{2,p}\right)x_{1,p}$, (1)

Lipid: $\frac{dx_{1,l}}{dt} = -\left(k_{1,l} + k_{2,l}\right)x_{1,l}$, (2)

Carbohydrate: $\frac{dx_{1,c}}{dt} = -\left(k_{1,c} + k_{2,c}\right)x_{1,c}$, (3)

Aqueous-phase products: $\frac{dx_2}{dt} = -(k_4 + k_5)x_2 + k_{1,p}x_{1,p} + k_{1,l}x_{1,l} + k_{1,c}x_{1,c} + k_3x_3$, (4)

Biocrude: $\frac{dx_3}{dt} = -(k_3 + k_6)x_3 + k_{2,p}x_{1,p} + k_{2,l}x_{1,l} + k_{2,c}x_{1,c} + k_4x_2'$, (5)

Gas: $\frac{dx_4}{dt} = k_5x_2 + k_6x_3$, (6)

where x refers to the mass fraction and k represents the reaction rate constants. The reaction rate constants are interpolated according to values at temperatures from 250 °C to 400 °C, as shown in Table 3. The values of reaction rate constants are assumed to be zero at 0 °C.

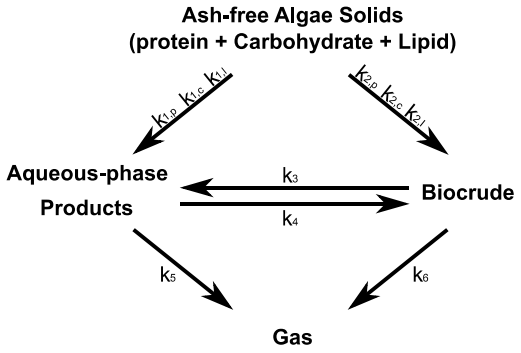

Fig. 4 Reaction kinetics (Valdez et al., 2014).

Table 3 Values of reaction rate constants (Valdez et al., 2014).

k (min^{-1})	250 °C	300 °C	350 °C	400 °C
$k_{1,p}$	0.095	0.20	0.28	0.33
$k_{1,l}$	0.15	0.35	0.35	0.35
$k_{1,c}$	0.25	0.35	0.35	0.35
$k_{2,p}$	0.13	0.13	0.28	0.32
$k_{2,l}$	0.031	0.11	0.33	0.35
$k_{2,c}$	0.00010	0.00010	0.0010	0.0032
k_3	0.0044	0.14	0.30	0.35
k_4	0.003	0.12	0.26	0.26
k_5	0.00010	0.00040	0.0014	0.0014
k_6	0.00010	0.00020	0.00090	0.0053

3 Results and discussion

3. 1 Comparison with a batch reactor result

Figure 5 presents the comparison of the calculated mass fractions of ash-free algae solids, aqueous-phase products, biocrude and gas with time. Here the ash-free algae solids are comprised of proteins, lipids and carbohydrates. The predicted mass fraction of the products are compared with the experimental data in the literature (Valdez et al., 2014). Note that the experimental data was obtained using a batch reactor, while a coil reactor was adopted in the current simulation. Figure 5 shows that the predicted mass fractions of these four components are close to that of the measured mass fractions in the batch reactor (Valdez et al., 2014) at the 10^{th} minute.

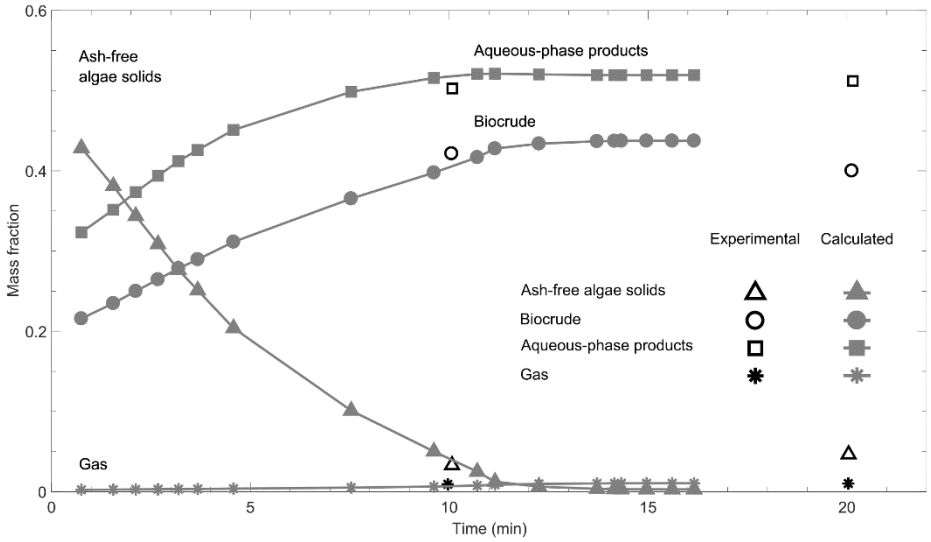

Fig. 5 Comparison of measured (Valdez et al., 2014) and predicted mass fractions of ash-free algae solids, aqueous-phase products, biocrude and gas.

3. 2 Influence of thermal properties on the HTL process in the coil reactor

Fig. 6 and Fig. 8 present the predicted mass fraction of the reactants and the three products of the HTL slurry for various values of heat conductivity and heat capacity for each of the components in the HTL reaction, respectively. It can be seen that, in the current simulations, compared with the reference conditions (Table 1), the predicted mass fraction of the components are all independent of whether the thermal conductivity or heat capacity of each component is increased or decreased by a factor of three . The same trend can be observed in the predicted values of residence time, as shown in Fig. 7 and Fig. 9. These imply that, for the reaction kinetics of Valdez et al. (2014), the thermal property values used have no obvious influence on the prediction of the mass fraction of the components in the coil HTL reactor. Similarly, when predicting the mass fraction and residence time of each component in the reaction, no influence of the molar mass value was observed, as shown in Fig. 10 and Fig. 11, respectively.

It is important to note that the observed insignificant effects of the heat conductivity and the heat capacity on this lab-scale HTL reactor may not necessarily extend to other, larger-scale reactors. The diameter of the current coil reactor (6.35 mm) seems to be sufficiently small for heat conductivity and the heat capacity to not significantly affect the heat transfer in the radial direction in the developing part of the flow. However, for large-scale HTL reactors with a significantly larger diameter than assessed here, the heat conductivity and heat capacity may have a greater influence on the heat transfer in the radial direction and consequently on the HTC reactions. It is therefore recommended that a similar sensitivity campaign should be conducted for different HTC reactor designs.

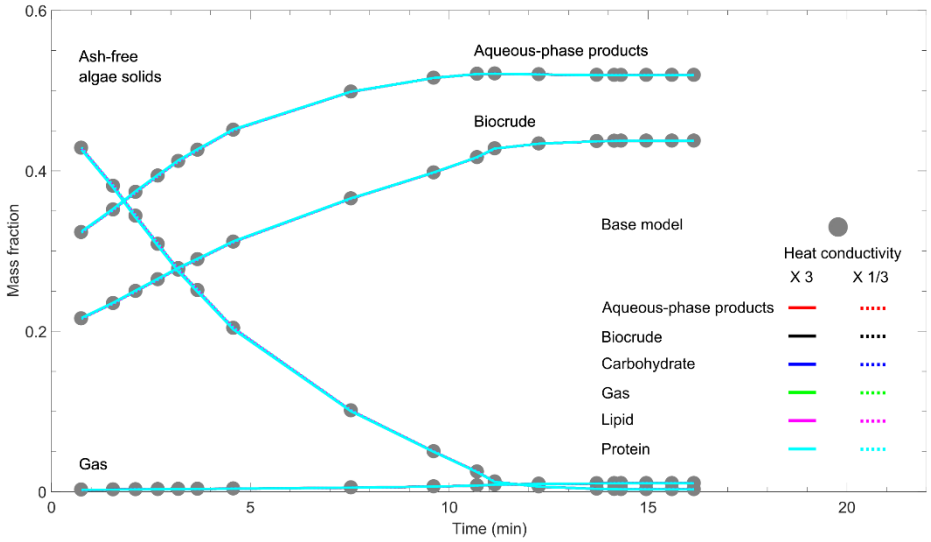

Fig. 6 Predicted mass fractions as a function of time for ash-free algae solids, aqueous-phase products, biocrude and gas using various assumed values of heat conductivity for each component in the reaction. (Note: only one line can be seen because the data lie exactly on top of each other).

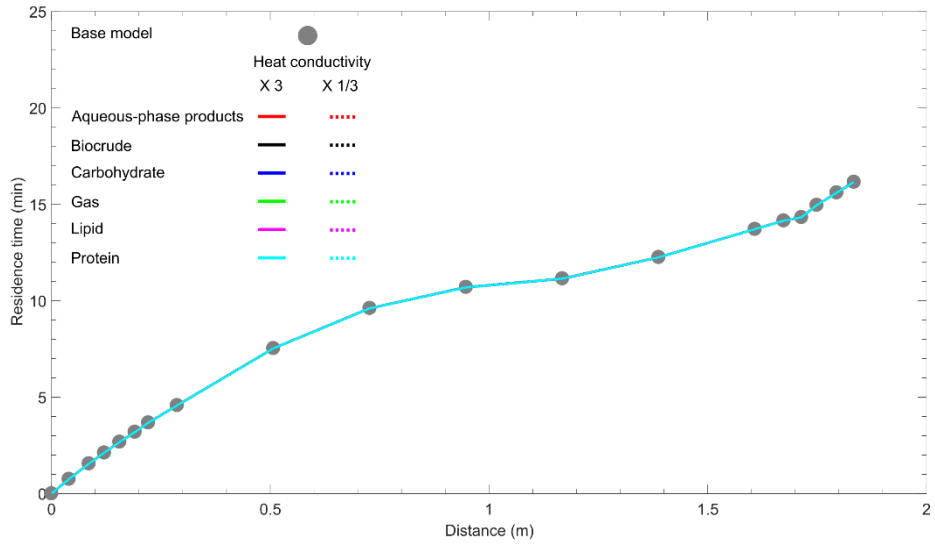

Fig. 7 Predicted residence time as a function of distance for a series of values of heat conductivity of each component in the reaction.

(Note: only one line can be seen because the data lie exactly on top of each other).

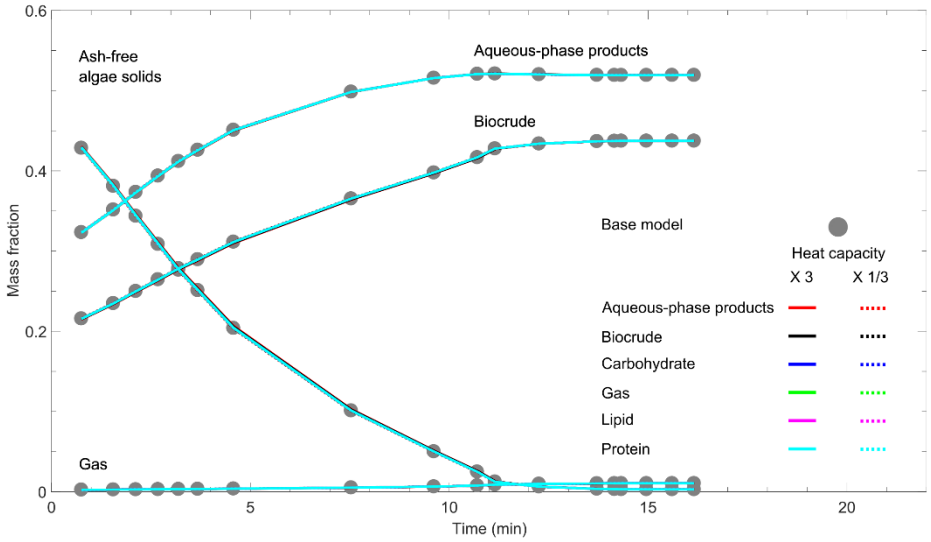

Fig. 8 Predicted mass fractions of ash-free algae solids, aqueous-phase products, biocrude and gas using different values of heat capacity of each component in the reaction.

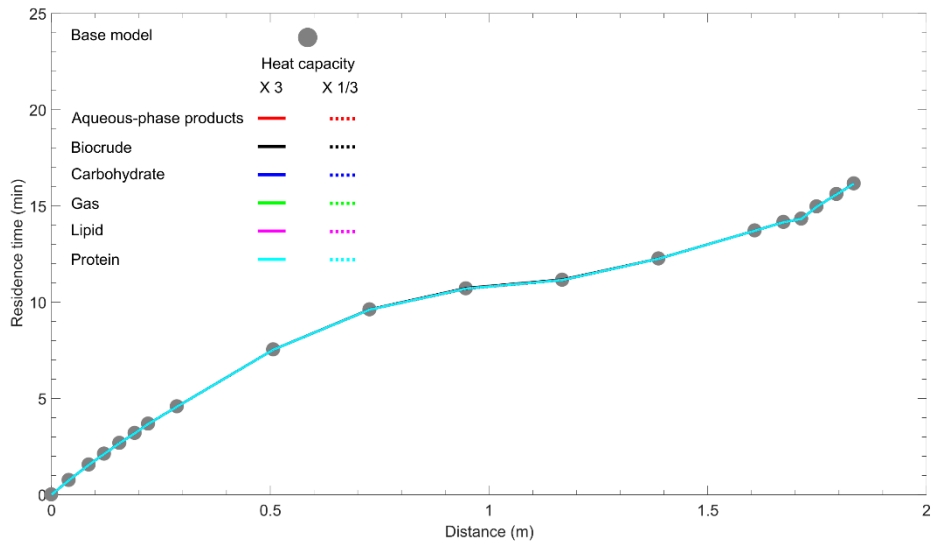

Fig. 9 Predicted residence time using different values of heat capacity of each component in the reaction.

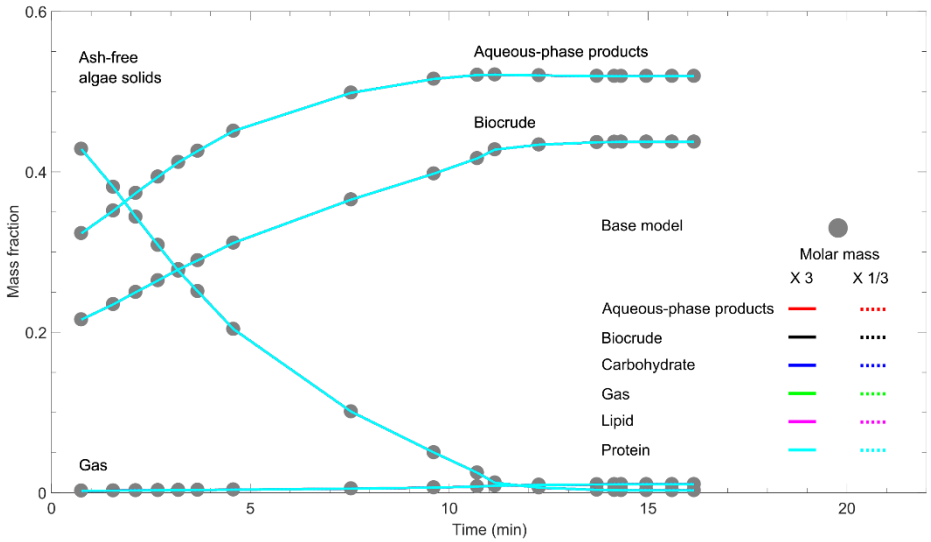

Fig. 10 Predicted mass fractions of ash-free algae solids, aqueous-phase products, biocrude and gas using different values of molar mass of each component in the reaction.

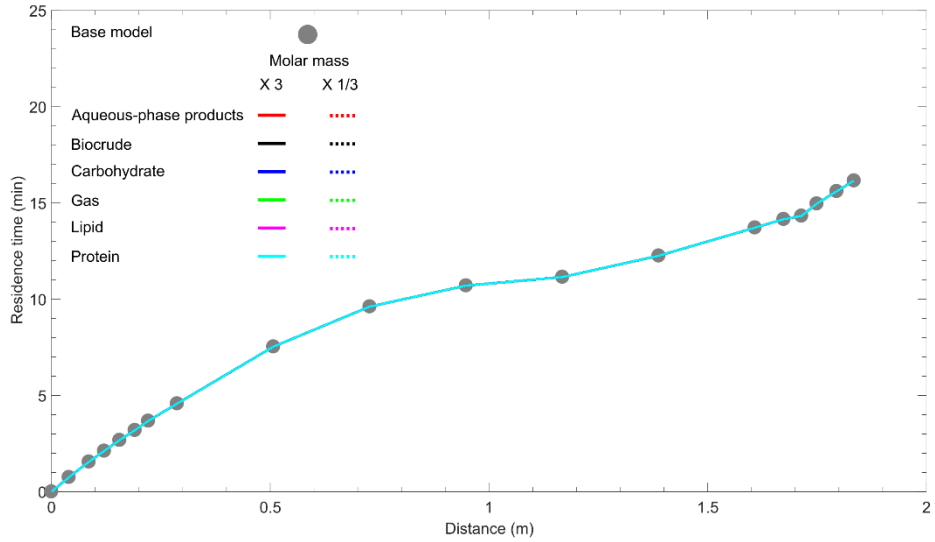

Fig. 11 Predicted residence time using different values of molar mass of each component in the reaction.

3. 3 Influence of viscosity on the HTL process in the coil reactor

Fig. 12 presents the predicted mass fraction of the reactants and the three products (biocrude, gas and aqueous-phase products) with various values of viscosity for the components, while the predicted residence time is shown in Fig. 13. As shown in Fig. 12, from about 3 minutes downstream the inlet, the variation rates of the mass fraction of the ash-

free algae solids and the three products are greater for the cases with lower viscosity of the components, particularly to reductions in viscosity of the proteins. That is, reducing the viscosity of the protein significant enhances the reaction (see the light blue dashed line). This suggests that the reactions are mixing limited. That is, reducing viscosity increases the rate of mixing between the reactants, which enhances the rate of reactions. Furthermore, the reactants with lower viscosity flow faster, which will increase the heat transfer over the base case and cases with higher viscosity. Table 3 shows that values of the reaction rate increase with the temperature, which causes the reaction rate of the components to increase, according to Equations 1-6.

Fig. 13 shows that the predicted residence time for the cases with a higher viscosity of a single component are greater than that for both the base case and those cases with a lower viscosity. This is because an increase in the viscosity of any component will reduce the convective transport of that component, and therefore its residence time. It is also interesting to note that further increasing the viscosity of the reactants and products over the base case has less influence on their mass fractions than decreasing their viscosities.

Further evidence of the importance of viscosity can be observed in the predicted distribution of residence times at the cross-sectional plane P12, which changes with the viscosity of biocrude, as shown in Fig. 14. Due to the friction of the reactor wall, the flow velocity of the slurry in the near wall region is expected to be slower than that in the central region, leading to longer residence times in the near wall region for all the three cases. The residence time is higher in the near wall region on the left hand side in this figure, which is because the left hand side is the inner side of the coil where the slurry velocity is lower. The predicted mean residence time at plane P12 for the case with the greatest viscosity of biocrude is longer than the other two cases with lower viscosities, as shown in Fig. 14.

Fig. 15 presents the probability density function (pdf) of the predicted residence time at plane P12 for the three cases with varying probability of biocrude. The predicted residence time in most of the areas of plane P12 is approximately 10 minutes, for all the three cases, while the probability that the predicted residence time is longer than 20 minutes for the case with the highest viscosity of biocrude, is greater than that for the other two cases. This trend is consistent with that shown in Fig. 13 and Fig. 14.

As shown in Fig. 12 and Fig. 13, the predicted outputs are most sensitive to the adopted value of viscosity of protein than to any other components. This is true for the predicted values of mass fraction of each component and the residence time.

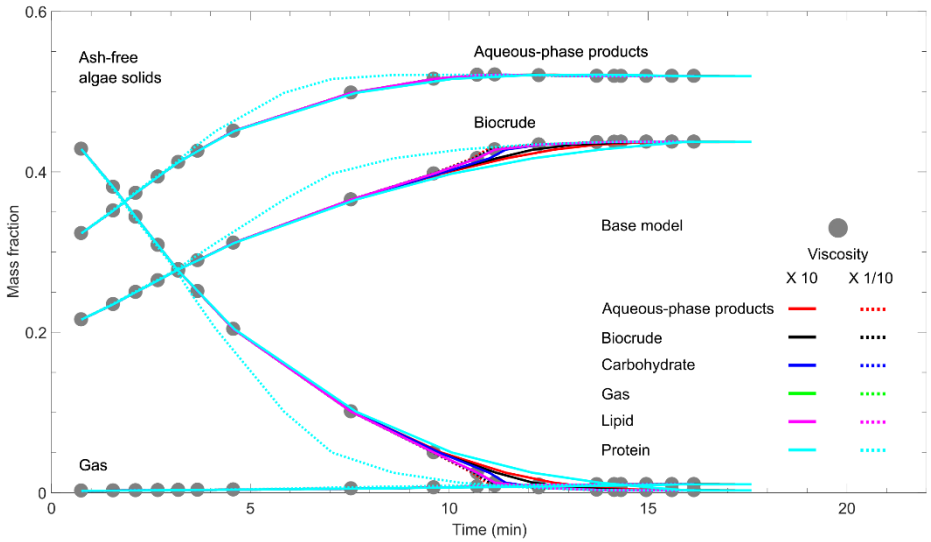

Fig. 12 Predicted mass fractions of ash-free algae solids, aqueous-phase products, biocrude and gas using different values of viscosity of each component in the reaction.

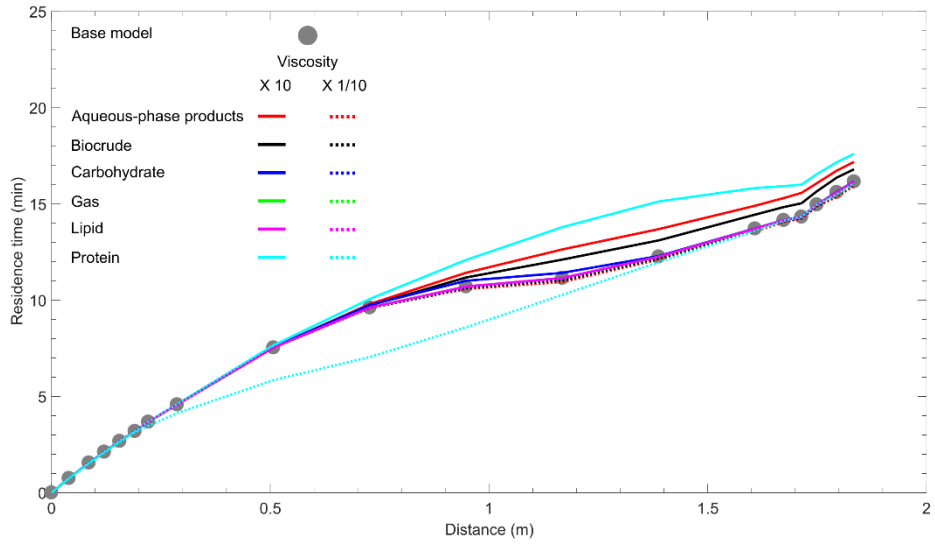

Fig. 13 Predicted residence time using different values of viscosity of each component in the reaction.

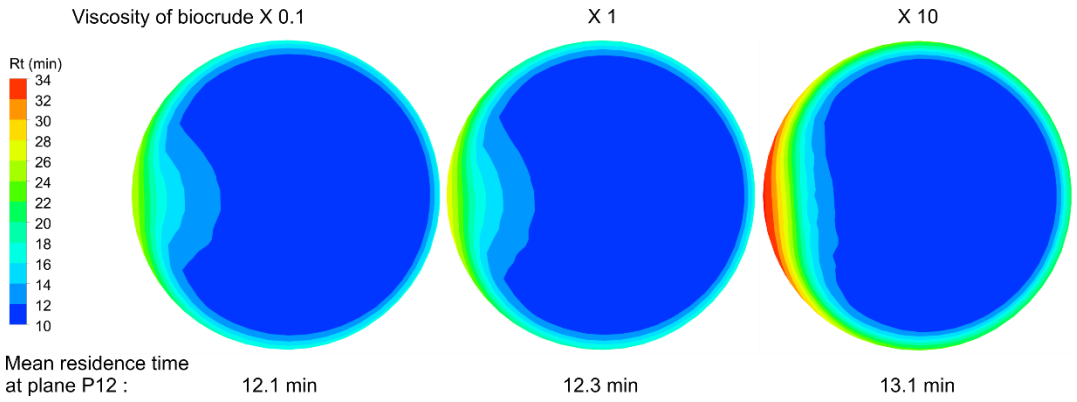

Fig. 14 Predicted residence times at cross sectional plane P12 in the cases with the variation of the viscosity of biocrude. Refer to Fig. **3** for the location of plane P12.

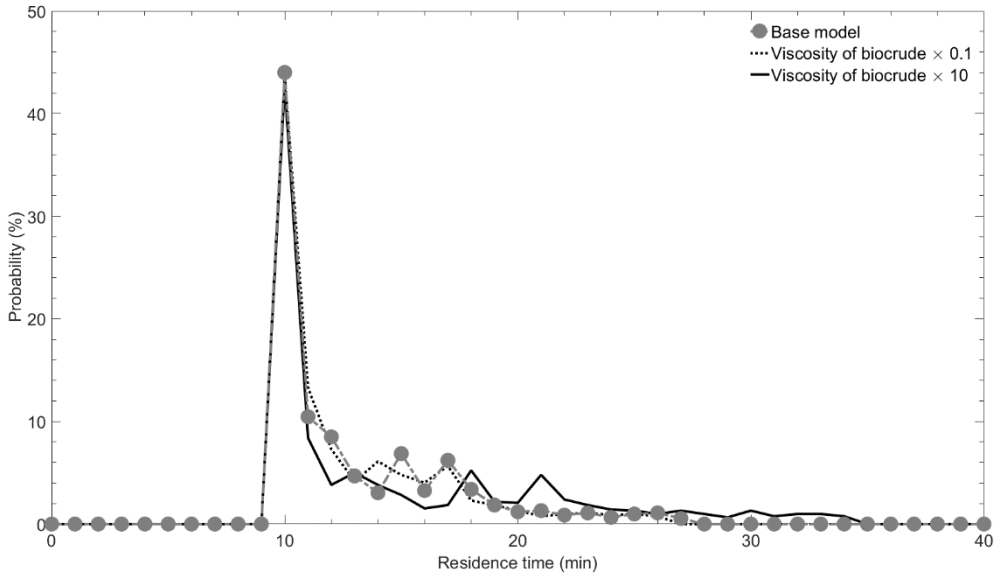

Fig. 15 Probability density function of the predicted residence times of the slurry at the cross-sectional plane P12 in the three cases with varying viscosity of biocrude. Refer to Fig. **3** for the location of plane P12.

4 Conclusions

A CFD model of a coil type HTL reactor has been developed based on the values for HTL reaction kinetics reported in the literature (Valdez et al., 2014). The CFD model is applied to assess the relative significance of the results to assumed values of heat conductivity, heat capacity, molar mass, and viscosity of both the reactants and products on the HTL reaction in terms of residence time and mass fractions. It is found that, for this relatively small coil reactor, the values of heat conductivity, heat capacity and molar mass have negligible effects on the HTL reaction. However,

the viscosity, particularly of the dominant reactants such as the proteins, was found to have a significant influence on the residence time and mass fractions, particularly when the viscosity of protein is reduced from values of the base case.

These results suggest both that the reactions are mixing limited, at least for the conditions of the relatively small reactor considered here, and also that further measurements of viscosity of the components are particularly important for advancing reliable prediction of the HTL technology. Also, while the findings of the paper are valid for the present lab-scale coil reactor, further analysis is also needed for other reactors, particularly at larger scale.

Acknowledgements

This work was supported by Southern Oil Refining and the Australian Research Council's Linkage Project funding scheme [Project LP150101241].

References

Barreiro, D.L., Prins, W., Ronsse, F., Brilman, W. 2013. Hydrothermal liquefaction (HTL) of microalgae for biofuel production: state of the art review and future prospects. *Biomass and Bioenergy*, **53**, 113-127.

Biller, P., Ross, A. 2011. Potential yields and properties of oil from the hydrothermal liquefaction of microalgae with different biochemical content. *Bioresource technology*, **102**(1), 215-225.

Billing, J., Anderson, D., Hallen, R., Hart, T., Maupin, G., Schmidt, A., Elliott, D. 2016. Design, fabrication, and testing of the modular hydrothermal liquefaction system (MHTLS). in: *2016 Symposium on Thermal and Catalytic Sciences for Biofuels and Biobased Products*. University of North Carolina-Chapel Hill.

Chen, H., Fu, Q., Liao, Q., Xiao, C., Huang, Y., Xia, A., Zhu, X. 2020. Modeling for thermal hydrolysis of microalgae slurry in tubular reactor: microalgae cell migration flow and heat transfer effects. *Applied Thermal Engineering*, **180**, 115784.

Chiaramonti, D., Prussi, M., Buffi, M., Rizzo, A.M., Pari, L. 2017. Review and experimental study on pyrolysis and hydrothermal liquefaction of microalgae for biofuel production. *Applied Energy*, **185, Part 2**, 963-972.

Chinnici, A., Arjomandi, M., Tian, Z., Nathan, G. 2016. A novel solar expanding-vortex particle reactor: experimental and numerical investigation of the iso-thermal flow field and particle deposition. *Solar Energy*, **133**, 451-464.

Chinnici, A., Tian, Z.F., Lim, J.H., Nathan, G.J., Dally, B.B. 2019. Thermal performance analysis of a syngas-fuelled hybrid solar receiver combustor operated in the MILD combustion regime. *Combustion Science and Technology*, **191**(1), 2-17.

Eboibi, B.E., Lewis, D.M., Ashman, P.J., Chinnasamy, S. 2015. Integrating anaerobic digestion and hydrothermal liquefaction for renewable energy production: an experimental investigation. *Environmental Progress & Sustainable Energy*, **34**(6), 1662-1673.

Elliott, D.C., Biller, P., Ross, A.B., Schmidt, A.J., Jones, S.B. 2015. Hydrothermal liquefaction of biomass: developments from batch to continuous process. *Bioresource technology*, **178**, 147-156.

Fu, Q., Chen, H., Liao, Q., Huang, Y., Xia, A., Zhu, X., Xiao, C., Reungsang, A., Liu, Z. 2018. Drag reduction and shear-induced cells migration behavior of microalgae slurry in tube flow. *Bioresource technology*, **270**, 38-45.

Fu, Q., Xiao, C., Huang, Y., Liao, Q., Xia, A., Chen, H., Zhu, X. 2020. Numerical study of flow and heat transfer characteristics of microalgae slurry in a solar-driven hydrothermal pretreatment system. *Applied Thermal Engineering*, **164**, 114476.

Hu, H., Jing, J., Tan, J., Yeoh, G.H. 2020. Flow patterns and pressure gradient correlation for oil–water core–annular flow in horizontal pipes. *Experimental and Computational Multiphase Flow*, **2**(2), 99-108.

Jena, U., Das, K.C. 2011. Comparative Evaluation of Thermochemical Liquefaction and Pyrolysis for Bio-Oil Production from Microalgae. *Energy & Fuels*, **25**(11), 5472-5482.

National Institute of Standards and Technology. 2005. Thermophysical Properties of Fluid Systems. in: *NIST Chemistry WebBook, SRD 69*. The United States of America.

Obeid, R., Lewis, D., Smith, N., van Eyk, P. 2019. The elucidation of reaction kinetics for hydrothermal liquefaction of model macromolecules. *Chemical Engineering Journal*, **370**, 637-645.

Patel, B., Hellgardt, K. 2015. Hydrothermal upgrading of algae paste in a continuous flow reactor. *Bioresource technology*, **191**, 460-468.

Ranganathan, P., Savithri, S. 2018. Computational Fluid Dynamics Simulation of Hydrothermal Liquefaction of Microalgae in a Continuous Plug-Flow Reactor. *Bioresource technology*.

Ross, A.B., Biller, P., Kubacki, M.L., Li, H., Lea-Langton, A., Jones, J.M. 2010. Hydrothermal processing of microalgae using alkali and organic acids. *Fuel*, **89**(9), 2234-2243.

Tian, Z., Witt, P., Schwarz, M., Yang, W. 2017. Numerical modelling of pulverised coal combustion. in: *Handbook of Multiphase Flow Science and Technology, 2017 / Yeoh, G. (ed./s), Ch.14, pp.1-35*, Springer.

Tran, K.-Q., Håkansson, L., Trinh, T.T. 2017. CFD pre-study of Nozzle reactor for fast hydrothermal liquefaction. *Energy Procedia*, **142**, 861-866.

Valdez, P.J., Tocco, V.J., Savage, P.E. 2014. A general kinetic model for the hydrothermal liquefaction of microalgae. *Bioresource Technology*, **163**, 123-127.

Yeoh, G.H., Tu, J. 2019. *Computational techniques for multiphase flows*. Butterworth-Heinemann.